

Quantum Fourier transform for quantum sensing

Vadim Vorobyov^{1,*}, Sebastian Zaiser¹, Nikolas Abt¹, Jonas Meinel¹, Durga Dasari¹, Philipp Neumann¹ and Jörg Wrachtrup^{1*}

¹ *3. Physikalisches Institut, IQST and Centre for Applied Quantum Technologies, and MPI for Solid State Research, University of Stuttgart, Pfaffenwaldring 57, 70569 Stuttgart, Germany*

Abstract

The Quantum Fourier Transformation (*QFT*) is a key building block for a whole wealth of quantum algorithms. Despite its proven efficiency, only a few proof-of-principle demonstrations have been reported. Here we utilize *QFT* to enhance the performance of a quantum sensor. We implement the *QFT* algorithm in a hybrid quantum register consisting of a nitrogen-vacancy (NV) center electron spin and three nuclear spins. The *QFT* runs on the nuclear spins and serves to process the sensor - NV electron spin signal. We demonstrate *QFT* for quantum (spins) and classical signals (radio frequency (RF)) with near Heisenberg limited precision scaling. We further show the application of *QFT* for demultiplexing the nuclear magnetic resonance (NMR) signal of two distinct target nuclear spins. Our results mark the application of a complex quantum algorithm in sensing which is of particular interest for high dynamic range quantum sensing and nanoscale NMR spectroscopy experiments.

INTRODUCTION

The Quantum Fourier transform (QFT) is a key element in a variety of quantum algorithms, such as conventional phase estimation, Shor's prime factorization protocol [1], period and order finding [2], or in the modern applications of quantum machine learning [3]. Along with the large theoretical research triggered in the fields of physics, chemistry and computer sciences over the past two decades, there have been experimental demonstrations of the algorithm using various physical systems involving superconducting qubits [4], trapped ions [5], nuclear magnetic resonance (NMR) [6], and integrated optics [7]. Yet, besides these proof-of-principle demonstrations no practical use of the QFT in e.g. factorization of large numbers has been made, because it would require a so far not available number of qubits.

On the other hand, classical Fourier transformation is used in a much larger variety of applications than the ones highlighted above for QFT. Excellent examples are found in signal analysis, specifically in spectroscopy, where in e.g. infrared and particularly in nuclear magnetic resonance, fast Fourier transformation (FFT) is the hallmark of modern biomolecular nuclear magnetic resonance structure analysis. In this technique signal post processing is used to demultiplex a complex multifrequency signal essentially yielding a massive reduction in signal acquisition time over measuring each frequency separately. Here we show, that using a multiqubit sensor and QFT simultaneously can demultiplex a multifrequency signal in situ and yield superior sensor performance.

In a typical quantum sensing scenario a physical quantity α which gives rise to the energy shift $\delta E(\alpha)$ and leads to the phase accumulation $\phi = \delta E(\alpha) \cdot \tau$ of the quantum state used for the measurement. This phase shift is measured by e.g. Ramsey interferometry [8]. The measurement sensitivity scales with the phase acquisition time τ as $1/\sqrt{\tau}$ in the standard quantum limit. In case multiple $\delta E(\alpha_i)$ are detected, for example caused by a complex nuclear magnetic resonance spectrum, the acquired phase would comprise multiple phases ϕ_i . To yield an unambiguous phase readout, the phase evolution is restricted to the interval $[0, \pi]$, when using a single sensor spin for phase measurements. Since the acquired phase $\phi = \sum_i \phi_i = \tau \sum \delta E(\alpha_i)$, is given by the evolution time τ multiplied with the sum of all frequency components, the maximum acquisition time is thus determined by the largest spectral component, significantly reducing the overall sensitivity. The addition of multiple memory and register qubits and use of QFT allows to extend the dynamic range and hence

sensitivity in such measurement and to demultiplex the individual harmonics from individual sources (spins) onto various memories outputs as depicted on Fig. 1.

We implement the *QFT* algorithm on a three nuclear ancillary spin register coupled to nitrogen vacancy (NV) center in diamond and demonstrate phase digitization. Further we use this to perform high dynamic range sensing of a RF signal and parallel correlation spectroscopy of two distinct weakly coupled target spins. We show here, that extending the dynamic range of the sensor by encoding the acquired phase ϕ into memory states $|m_1 m_2 \dots\rangle$, and using the *QFT* algorithm to demultiplex the signal harmonics also enhances the overall sensitivity of the sensor.

RESULTS

Implementation of QFT algorithm

Our *QFT* algorithm utilizes an electron spin as sensor to acquire a phase ϕ which we subsequently transfer onto memory and processing qubits to perform a *QFT*, the result of which is read out after the phase acquisition is accomplished [2]. To implement our experiment we use a single electron spin of an NV center in diamond with long coherence time at room temperature as a probe qubit capable of sensing various external quantities [9–11]. As memory register we use three well isolated and thus long-lived individual nearby nuclear spins (^{14}N , $^{13}\text{C}_1$, $^{13}\text{C}_2$) which form a twelve level quantum system for storage and processing of the sensed information as schematically depicted in Fig. 1a. We note that we can perform single-shot readout on all three nuclear spins. The electron spin sensor measures small magnetic fields and distributes the phase acquired during the sensing step U^{2^i} to the i^{th} memory qubit (see Fig. 1. (b), (c)). The long lifetime of the memories allows for long phase storage and consequently high spectral resolution due to large correlation times. In our setting, α is a magnetic field created by proximal target spins or a classical signal, or for example nuclear spins of an unknown complex molecule or spin cluster. In the case of a nuclear spin-bath, the multi-frequency signal from the sample with peak frequencies f_1 and f_2 and amplitudes a_1 and a_2 results in a beating in the free precession signal of the nuclear spins. The task at hand is to demultiplex this by applying Quantum Fourier transformation.

In case of our hybrid qubit-qutrit register the *QFT* is similar to a standard register

composed of qubits i.e. realized with use of the Hadamard and control rotation gates. Fig. 1e shows a circuit representation of a QFT and QFT^\dagger algorithm for an effective twelve level system, consisting of one qutrit and two qubits (see Supplementary). In general, the QFT involves local Hadamard (Chrestenson [12]) gates for qubits (qutrit) and a large number ($O(n^2)$) of conditional non-local rotational gates, and are implemented using optimal control (see Supplementary) to enhance fidelity.

In the version of the algorithm adapted to our hybrid qubit-qutrit quantum register (see Fig. 1c) the register spins are initialized in a superposition initial state $|+\rangle$ with zero phase using local Hadamard and Chrestenson gates. After that, the sensor interacts with the target system, attains phase information and stores it onto the register spins using controlled U^i gates [13]. The phase acquisition gate \hat{U} in Fig. 1b,c presents a unitary operator acting on the electron spin for example by $\hat{U}_e = \exp\{i \sum_{t_i} A_{zz}^i S_z I_z^i \tau\}$ or $\hat{U}_e = \exp\{i \sum_{t_i} A_{zx}^i S_z I_x^i \tau\}$, depending on the control sequence and on the state of the target spin system. Finally, QFT^\dagger transforms the acquired phases to a bit representation (digitization) by mapping it onto populations of the nuclear spin register which are then either used as a classical memory during the correlation time or read out through a single-shot measurement [14].

In a classical Fourier transformation of e.g. an NMR signal, the data is acquired first and then the Fourier transformation is applied subsequently. Applying the QFT however, requires a simultaneous recording of data and performing QFT^\dagger . We start by first applying the QFT on the initialized nuclear quantum register and then transfer the measured phases from the electron spin to the nuclear quantum bits. The role of QFT^\dagger on the nuclear quantum register is to make the mapping of acquired phases during the phase acquisition more efficient by realizing an unambiguous digitization of the phase. To demonstrate the efficiency of this step and compare QFT with other phase conversion methods, we first prepare the initial state of the register with a certain phase ϕ mimicking a phase acquired by the sensor spin (see Fig. 2)(see Supplementary). The figure shows the result of a readout of the nuclear register (i.e. its bit values) for different input phases. The simplest way to convert this phase into a detectable I_z magnetization are Hadamard gates on each nuclear spin which rotate the spin from the phase plane into the z direction. For comparison we show the result of the same initial state of the nuclear spins with the QFT^\dagger protocol. As apparent from the upper row of Fig. 2. b,c the application of local gates results in quantum register readouts scattered throughout the whole logical space. Most importantly, most

phases (except $\phi = \pi$) result in multiple bit values, i.e. the register readout does not result in an unambiguous phase. On top, the readout contrast is reduced by $1/a$, when a is the number of bit value results per given phase. However, the contrast is maintained upon application of the QFT^\dagger , and the measurement output corresponds to a well defined phase. In Fig. 2b,c the analytical and experimental result for the application of $H^{\otimes 3}$ and QFT^\dagger on the same initial phase encoded state is shown respectively. Besides the excellent agreement between experiment and theory the results show excellent fidelity of our QFT based protocol for sensing with hybrid quantum devices containing multi-qubit registers (see Supplementary). For the QFT based protocol, the fidelity stays constant over the whole range of ϕ , and the individual qubits are projected onto their eigen basis, minimizing the spin projection noise during the projective readout of the register state. A further advantage of the QFT is that in previous application of in-situ correlation

In classical Fourier transform NMR, a multifrequency signal is recorded in a Ramsey-type experiment and its frequency components are subsequently determined by a Fourier transformation. In our implementation we measure an oscillating magnetic field and process the QFT in-situ (see Fig. 3a). A notable difference between the classical approach and our quantum sensor is that we first need to convert the frequency of the oscillating field into a phase which can be transferred to the nuclear quantum register. To accomplish this, we design and implement phase gates U^i , converting the AC magnetic field into a phase acquired by the electron spin of NV center and imprint it onto various nuclear register qubits [15]. Essentially, U^i comprises a train of phase inversion pulses which are commensurate with the oscillation of the AC magnetic field sandwiched between two CNOT gates which write the phase on the nuclear register (see Fig. 3b). Our measurement starts with memory initialization, followed by a sensing stage. In the sensing stage, the sensor qubit attains phase information related to the incident magnetic field and swaps it onto the memory qubits where it is stored in form of a relative phase and is transformed through the QFT^\dagger into a binary representation, which is then finally read out. Fig. 3c shows the output of the QFT^\dagger in the register states basis representation $|m_1m_2m_3\rangle$. Analogous to Fig. 2c, the image shows the unambiguous representation of the field amplitude with respect of the measurement result output, which corresponds to full 2π phase estimation range on the twelve-level quantum register. We would like to highlight here the enhanced dynamic range of the QFT alongside the precision of the sensing protocol. As the DR scales with

the dimension of the Hilbert space (see Supp. for details) we experimentally find a $\sim 12x$ improvement when compared to the single qubit case. To see the benefit of using a *QFT* based phase estimation we analyse the Fisher information in Fig. 3.d and use it to visualize the scaling behavior of our phase estimation scheme with respect to the number of qubit resources used. To do this we analyze the output state in the sensing protocol as a function of the acquired phase ϕ , using the expression for the Fisher information for the pure states, viz., $F_q = 4(\langle \partial_a \psi | \partial_a \psi \rangle - |\langle \partial_a \psi | \psi \rangle|^2)$. We estimate the theoretical Fisher information of the final state of the sensing protocol with respect to parameter ϕ , and compare it to the expressions obtained for the case of n non-entangled qubits, and n fully entangled qubits (NOON states), which represents the Standard Quantum limit and Heisenberg scaling limit in number of used qubit resources (see Supplementary). In the same plot we show the experimentally achieved values of the Fisher information for the case of a twelve-level register. These values were estimated for the experiment shown in Fig. 2 and Fig. 3 for the bare *QFT*[†] and *QFT*[†] with sensing. While the experimental values show a slight deviation in the achievable information compared to the theoretically calculated case, they outperform the Standard Quantum Limit and approach Heisenberg scaling (see Methods).

Finally we turn to measuring signals of multiple, non-identical nuclear spins. State-of-the-art quantum sensing protocols with NV centers in diamond enable high resolution nuclear magnetic resonance experiments reaching sub Hz resolution. This is either accomplished by measuring the signal in subsequent measurements and correlating them afterwards [16, 17], or by in-situ correlation spectroscopy [15, 18]. In the latter first the oscillating magnetic field caused by the Larmor precession of the target nuclei is converted into a phase, similar to the above detection of the test field. However, the phase detection sequence is repeated after a certain (correlation) time T_c to achieve a higher frequency resolution [19].

Here we extend this method by a multi-qubit memory and apply *QFT* on these qubits. The general working principle of this method is depicted schematically in Fig. 4a. It is using multiple nuclear spins to store the phase of the electron spin and in addition is applying *QFT* to the attained data. The protocol starts with applying a *QFT* to the initialised nuclear spin register. Subsequently the NMR signal of the target spins is measured by the electron spin and its phase information is encoded in the nuclear spin register. A *QFT* algorithm is then applied to these nuclear spin quantum states, essentially encoding the phase information into nuclear spin eigenstates for long time storage. Arbitrary operations could be done on

the target spins during that period, for example a Ramsey sequence or a single π pulse, before the memory is mapped back for the second correlation step. The operations on the target nuclear spins change the local magnetic field of the sensor electron spin. In the final decoding stage of the algorithm, this new magnetic field is compared (correlated) with the one measured during the encoding state. The addition of multiple register qubits is a natural choice for expanding the memory capacity and hence improve the function of the method. However, a proper way of processing the information is required and this is achieved by the *QFT*.

During the protocol, the *QFT* is used to demultiplex the signals originating from the mixture of target spins onto separate memories outputs. To demonstrate this we choose weakly coupled nuclear spins of ^{13}C with A_{zz} coupling of 6 kHz (t_1) and 12.4 kHz (t_2) as two target spins.

The *QFT* and *QFT*[†] in between the two sensing steps and the duration of interrogation time τ during phase accumulation was chosen such that the signal originating from the 12 kHz coupled target spin is reflected by the result measured on $^{13}\text{C}_{414}$ nuclear spin memory, whereas the signal originated by 6 kHz target spin is measured by the output of the another register qubit ($^{13}\text{C}_{90}$)(see Supplementary).

We perform correlation spectroscopy of these target spins with a Ramsey type measurement in between the sensing steps. For the nuclear spin Ramsey $\pi/2$ pulses, a frequency detuning of 2.5 kHz to the weaker coupled target spin was chosen, such that we should measure an oscillation with 2.5 kHz on $^{13}\text{C}_{90}$ and an oscillation of 3.8 kHz on the $^{13}\text{C}_{414}$ memory output, respectively. This is observed in the measurement and depicted in Fig. 4e-f achieving an NMR linewidth of 76 Hz and 68 Hz.

In our measurement protocol the phase acquisition is adjusted such, that the least significant qubit (LSQ) acquires a total phase $\phi_{LSQ} = 4 \cdot 2\tau A_{t_2} = 2\pi$ and the most significant qubit (MSQ) a phase of $\phi_{MSQ} = 4 \cdot \tau A_{t_2} = \pi$ as the stronger coupled target t_2 spin flips during the correlation time. The register acquires a phase $\phi_{LSQ} = 4 \cdot 2\tau A_{t_1} = \pi$ on the LSQ and $\phi_{MSQ} = 4 \cdot \tau A_{t_1} = 0(\text{mod}2\pi)$ on the MSQ when the weaker coupled target spin t_1 flips. Hence, we pick a sensing time τ , such that it fits the energy difference of the combined target spins. In our case, the sensing time τ was chosen to be $\tau = 3\pi/8 \cdot (A_{t_1} + A_{t_2})^{-1} \approx (4 \cdot 12\text{kHz})^{-1}$ as depicted in Fig. 4d.

This setting results in the mapping of phases acquired due to the signal of the individual

target spins as shown in Fig. 4d onto the register states. As a result when performing Ramsey type correlation measurement on two target spins their oscillation are directly mapped onto the output populations of memory spins which are single-shot readout in Fig. 4e. By performing an Fast-Fourier Transform (FFT) on the results of individual memory outputs we show two resonances corresponding to 12 and 6 kHz ^{13}C nuclear spins with the resolution of $\approx 70\text{Hz}$ depicted in Fig. 4f.

In conclusion we demonstrated the first implementation of QFT using individual solid-state nuclear spins in diamond. Combining QFT with sensing we extended the capability of diamond based quantum sensors and realized a multiqubit phase estimation circuit in a correlation spectroscopy measurements, and monitored the dynamics of a two target spin with high precision. Their NMR signals were demultiplexed and read out as a separate quantum register outputs. Our results show, that multiple qubit algorithms can be beneficial for quantum sensing, even in terms of sensitivity scaling.

It has been shown, that a NV register can comprise up to seven nuclear qubits, extending the number of frequencies simultaneously detected to a value which is of interest to be applied in multi species nanoscale NMR.

METHODS

NV center - nuclear spin system

In our experiments we use a single electron spin of an individual NV center as a sensor The electron spin has a long T_2 coherence time [15] at ambient conditions despite its large coupling to external fields and consequently a high intrinsic sensitivity. To perform the QFT , one needs highly controllable nuclear spins that constitute the memory register. The NV center has several hyperfine coupled nuclear spins in the environment having much longer coherence times as compared to the electron spin but having a low susceptibility to the environment. The NV center has several hyperfine coupled nuclear spins in the environment having much longer coherence times as compared to the electron spin but having a low susceptibility to the environment. The co-processor is formed using the strongly coupled (2.16 MHz) ^{14}N nuclear spin of the NV center, and two ^{13}C nuclear spins (labelled as $^{13}\text{C}_{414}$ and $^{13}\text{C}_{90}$) with hyperfine coupling along the quantization axis of the NV center $A_{zz} \approx 414\text{kHz}$ and $A_{zz} \approx 90\text{kHz}$

respectively [20]. It presents an effective 12-level system and allows to run a general set of quantum operations including the QFT algorithm. Additionally, our register allows for single-shot readout of nuclear spins and thus efficient extraction of sensing information [14, 20]. Due to the relatively strong hyperfine coupling we can resolve all the twelve lines in the ODMR spectrum of the NV center which has an T_2^* time about 20 μs . This marks the key step of our protocol, as the digitized phase is encoded as populations among the 12-levels with a resolution of $\phi/12$. The individual addressing of these levels set the limit on our precision. Using strongly coupled nuclear spins as memory qubits allows them to be individually addressed and readout. (see Supplementary Information).

Precision and dynamic range scaling

For the multiple independent qubits the Quantum Cramer-Rao Bound (QCRB) gives the ultimate bound for precision of a parameter estimation. The formula for the QCRB reads $\Delta\phi_{SQL} = \frac{1}{\sqrt{N_m}\sqrt{F_q}} = \frac{1}{\sqrt{N_m}\sqrt{n}}$, where N_m is the number of measurements and n is the number of independent qubits. It is also worth noting that in a sensing scenario, when an unknown parameter α has to be determined, one can write that $\phi = \delta E(\alpha)\tau/h$. The corresponding final state reads as $|\psi\rangle = \frac{1}{\sqrt{2}}(|0\rangle + e^{i\frac{\delta E}{\hbar}\delta\alpha\tau/h}|1\rangle)$, and the Fisher Information with respect to the parameter α reads $F_\alpha^q = n\partial E_\alpha^2\tau^2$. $\Delta\alpha = h\frac{1}{\sqrt{N_m}}\frac{1}{\sqrt{n}\partial_\alpha E\tau}$ comprises the Standard Quantum limit in number of measurements and Heisenberg limit scaling in measurement time. It shows SQL limit scaling of precision in the number of independent qubits. When multiple independent qubits are subject to a phase estimation algorithm, the Fisher information in phase estimation reads $F_q = \sum_{j=0}^{n-1} 2^{2j} = 1/3(4^n - 1)$, the QCRB for phase $\Delta\phi_{PEA} = \frac{1}{\sqrt{N_m}}\frac{1}{\sqrt{(4^n-1)/3}} \approx \sqrt{\frac{3}{N_m}}\frac{1}{2^n}$ at large n and it reduces exponentially with number of used qubits. On the other side, when a phase is acquired due to the sensing, then $\phi = \tau\partial_\alpha E\delta\alpha/h$. In that case $F_\alpha^q = \sum_{j=0}^{n-1} (2^j\tau\partial_\alpha E/h)^2$, and $\Delta\alpha = h\sqrt{\frac{3}{N_m}}\frac{1}{2^n}\frac{1}{\tau\partial_\alpha E}$. Since the total time of the measurement is approximately $T \approx 2^n\tau$ then $\Delta\alpha = h\sqrt{\frac{3}{N_m}}\frac{1}{T\partial_\alpha E}$. In comparison, for the case of n entangled qubits as an initial state, when a similar phase estimation operation is applied, the Fisher information reads $F_q = (\sum_{j=0}^{n-1} 2^j)^2 = (2^n - 1)^2$. In the case of sensing a parameter α as in the previous case, $F_\alpha^q = (\sum_{j=0}^{n-1} 2^j\tau\partial_\alpha E)^2$, and $\Delta\phi_{HL} = \frac{1}{\sqrt{N_m}}\frac{1}{(2^n-1)}$, which

has an exponential scaling in number of qubits and for high n scales as for non-entangled qubits. The precision of sensing of a parameter is equal to $\Delta\alpha = h \frac{1}{\sqrt{N_m}} \frac{1}{(2^n - 1)} \frac{1}{\tau \partial_\alpha E}$. To summarize the QCRB gives the following scaling for the precision of conventional sensing using n non-interacting qubits, QPEA, and QPEA+Entangled state:

$$\Delta\alpha_{SQL} = h \frac{1}{\sqrt{N_m}} \frac{1}{\tau \partial_\alpha E} \quad (1)$$

$$\Delta\alpha_{QPEA} = h \sqrt{\frac{3}{N_m(4^n - 1)}} \frac{1}{\tau \partial_\alpha E} \quad (2)$$

$$\Delta\alpha = h \frac{1}{\sqrt{N_m}} \frac{1}{(2^n - 1)} \frac{1}{\tau \partial_\alpha E} \quad (3)$$

Dynamic range

In a quantum measurement the 2π periodicity of the acquired phase limits the measurement range $R_\alpha = \pi/(\partial_\alpha E \tau)$ over which the parameter α could be unambiguously determined. Thus there is a trade-off between the precision (Δ) and maximum range of the measurement (R), efficiently represented via a dynamic range ($DR = R/\Delta$). In a standard case of n qubit sensing using Ramsey type sequence $DR_{SQL} = \frac{\pi}{\tau \partial_\alpha E} / h \frac{1}{\sqrt{N_m}} \frac{1}{\tau \partial_\alpha E} = \frac{\pi}{h} \sqrt{N_m}$.

In the case of phase estimation algorithm with a *QFT* the maximum range is given by the smallest phase acquisition time τ and phase could be resolved in whole $0 - 2\pi$ range, while the precision is given by the longest phase acquisition time $\tau \cdot 2^n$. In that case $DR_{QPEA} = \frac{2\pi}{\tau \partial_\alpha E} / h \sqrt{\frac{3}{N_m(4^n - 1)}} \frac{1}{\tau \partial_\alpha E} = \frac{2\pi}{\sqrt{3}h} \sqrt{N_m} \sqrt{(4^n - 1)} \approx 2/\sqrt{3} DR_{SQL} \times 2^n$, where n is the number of qubits. In summary the phase estimation algorithm and *QFT* exponentially increase the dynamic range with the number of qubits in use.

* v.vorobyov@pi3.uni-stuttgart.de, j.wrachtrup@pi3.uni-stuttgart.de

- [1] P. W. Shor, “Algorithms for quantum computation: discrete logarithms and factoring,” in *Foundations of computer science* (S. Goldwasser, ed.), (Piscataway), pp. 124–134, IEEE Press, 1994.
- [2] M. A. Nielsen and I. L. Chuang, *Quantum computation and quantum information*. Cambridge university press, 2010.

- [3] J. Biamonte, P. Wittek, N. Pancotti, P. Rebentrost, N. Wiebe, and S. Lloyd, “Quantum machine learning,” *Nature*, vol. 549, pp. 195 EP –, 2017.
- [4] D. García-Martín and G. Sierra, “Five experimental tests on the 5-qubit ibm quantum computer,” *Journal of Applied Mathematics and Physics*, vol. 06, no. 07, pp. 1460–1475, 2018.
- [5] S. Debnath, N. M. Linke, C. Figgatt, K. A. Landsman, K. Wright, and C. Monroe, “Demonstration of a small programmable quantum computer with atomic qubits,” *Nature*, vol. 536, pp. 63 EP –, 2016.
- [6] Y. S. Weinstein, M. A. Pravia, E. M. Fortunato, S. Lloyd, and D. G. Cory, “Implementation of the quantum fourier transform,” *Physical Review Letters*, vol. 86, no. 9, pp. 1889–1891, 2001.
- [7] S.-H. Tan and P. P. Rohde, “The resurgence of the linear optics quantum interferometer — recent advances & applications,” *Reviews in Physics*, vol. 4, p. 100030, 2019.
- [8] N. F. Ramsey, “A molecular beam resonance method with separated oscillating fields,” *Physical Review*, vol. 78, no. 6, pp. 695–699, 1950.
- [9] F. Dolde, H. Fedder, M. W. Doherty, T. Nöbauer, F. Rempp, G. Balasubramanian, T. Wolf, F. Reinhard, L. C. L. Hollenberg, F. Jelezko, and J. Wrachtrup, “Electric-field sensing using single diamond spins,” *Nat Phys*, vol. 7, no. 6, 2011.
- [10] V. M. Acosta, E. Bauch, M. P. Ledbetter, A. Waxman, L.-S. Bouchard, and D. Budker, “Temperature dependence of the nitrogen-vacancy magnetic resonance in diamond,” *Phys. Rev. Lett.*, vol. 104, no. 7, p. 070801, 2010.
- [11] J. M. Taylor, P. Cappellaro, L. Childress, L. Jiang, D. Budker, P. R. Hemmer, A. Yacoby, R. Walsworth, and M. D. Lukin, “High-sensitivity diamond magnetometer with nanoscale resolution,” *Nature Physics*, vol. 4, pp. 810 EP –, 2008.
- [12] A. Al-Rabadi, L. Casperson, M. Perkowski, and X. Song, “Multiple-valued quantum logic,” 2002.
- [13] M. Pfender, N. Aslam, H. Sumiya, S. Onoda, P. Neumann, J. Isoya, C. A. Meriles, and J. Wrachtrup, “Nonvolatile nuclear spin memory enables sensor-unlimited nanoscale spectroscopy of small spin clusters,” *Nature Communications*, vol. 8, no. 1, p. 834, 2017.
- [14] P. Neumann, J. Beck, M. Steiner, F. Rempp, H. Fedder, P. R. Hemmer, J. Wrachtrup, and F. Jelezko, “Single-shot readout of a single nuclear spin,” *Science*, vol. 329, no. 5991, pp. 542–544, 2010.

- [15] S. Zaiser, T. Rendler, I. Jakobi, T. Wolf, S.-Y. Lee, S. Wagner, V. Bergholm, T. Schulte-Herbrüggen, P. Neumann, and J. Wrachtrup, “Enhancing quantum sensing sensitivity by a quantum memory,” *Nature Communications*, vol. 7, p. 12279, 2016.
- [16] S. Schmitt, T. Gefen, F. M. Stürner, T. Unden, G. Wolff, C. Müller, J. Scheuer, B. Naydenov, M. Markham, S. Pezzagna, J. Meijer, I. Schwarz, M. Plenio, A. Retzker, L. P. McGuinness, and F. Jelezko, “Submillihertz magnetic spectroscopy performed with a nanoscale quantum sensor,” *Science (New York, N.Y.)*, vol. 356, no. 6340, pp. 832–837, 2017.
- [17] D. R. Glenn, D. B. Bucher, J. Lee, M. D. Lukin, H. Park, and R. L. Walsworth, “High-resolution magnetic resonance spectroscopy using a solid-state spin sensor,” *Nature*, vol. 555, no. 7696, pp. 351–354, 2018.
- [18] A. Laraoui, F. Dolde, C. Burk, F. Reinhard, J. Wrachtrup, and C. A. Meriles, “High-resolution correlation spectroscopy of ^{13}C spins near a nitrogen-vacancy centre in diamond,” *Nat Commun*, vol. 4, p. 1651, 2013.
- [19] N. Aslam, “Nanoscale nuclear magnetic resonance with chemical structure resolution,” 2018.
- [20] G. Waldherr, Y. Wang, S. Zaiser, M. Jamali, T. Schulte-Herbrüggen, H. Abe, T. Ohshima, J. Isoya, J. F. Du, P. Neumann, and J. Wrachtrup, “Quantum error correction in a solid-state hybrid spin register,” *Nature*, vol. 506, no. 7487, 2014.

Acknowledgments We acknowledge financial support by the German Science Foundation (the DFG) via SPP1601, FOR2724, the European Research Council (ASTERIQS, SMel), the Max Planck Society, the Volkswagen Stiftung

Author Contributions

PN and JW developed the initial idea of the experiment. NA, SZ, VV, JM, PN and JW conducted the experiment. VV, DD, PN and JW performed the theoretical analysis. All authors contributed to the writing of the manuscripts.

Author Information

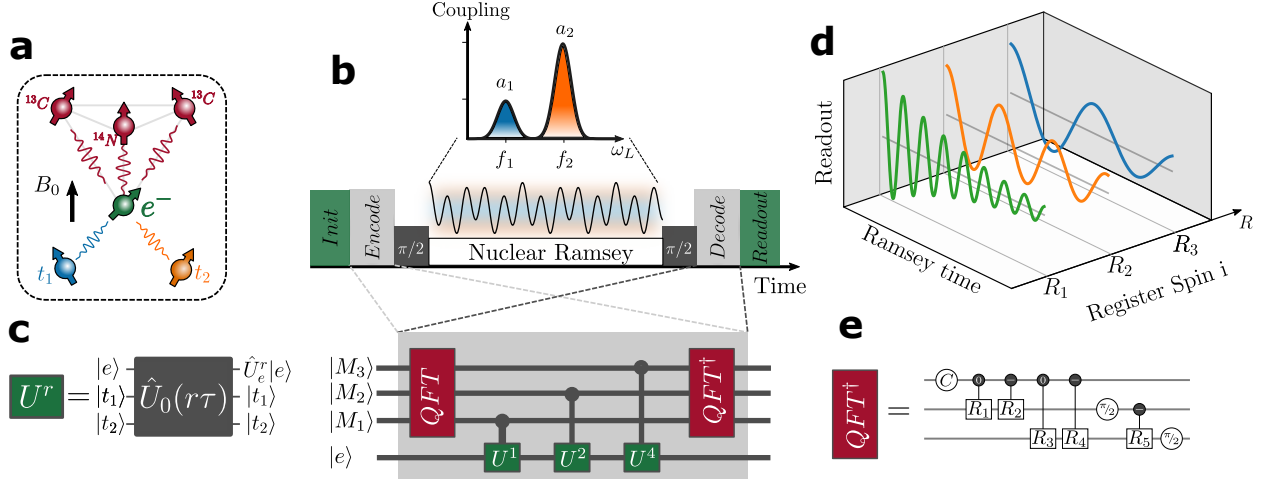


FIG. 1. (a) Schematic representation of the sensor consisting of a single sensor spin (green) which collects phase information of a distant target spin (blue and orange) and distributes it onto a local qubit register (red) made of one qutrit (^{14}N nuclear spin) and two qubits (^{13}C nuclear spins). (b) The target system spectrum, consisting of multiple frequencies f_1, f_2, \dots with corresponding amplitudes a_1, a_2, \dots with a schematic circuit for sensing of multiple target spins with implementation of QFT and QFT^\dagger . (c) The phase acquisition unitary gate for sensing of target nuclear spins t_1 and t_2 . (d) The readout result of the register qubits after performing measurements with the QFT algorithm. Each memory stores Ramsey oscillation of individual target nuclear spins. (e) QFT^\dagger quantum circuit for our hybrid quantum register

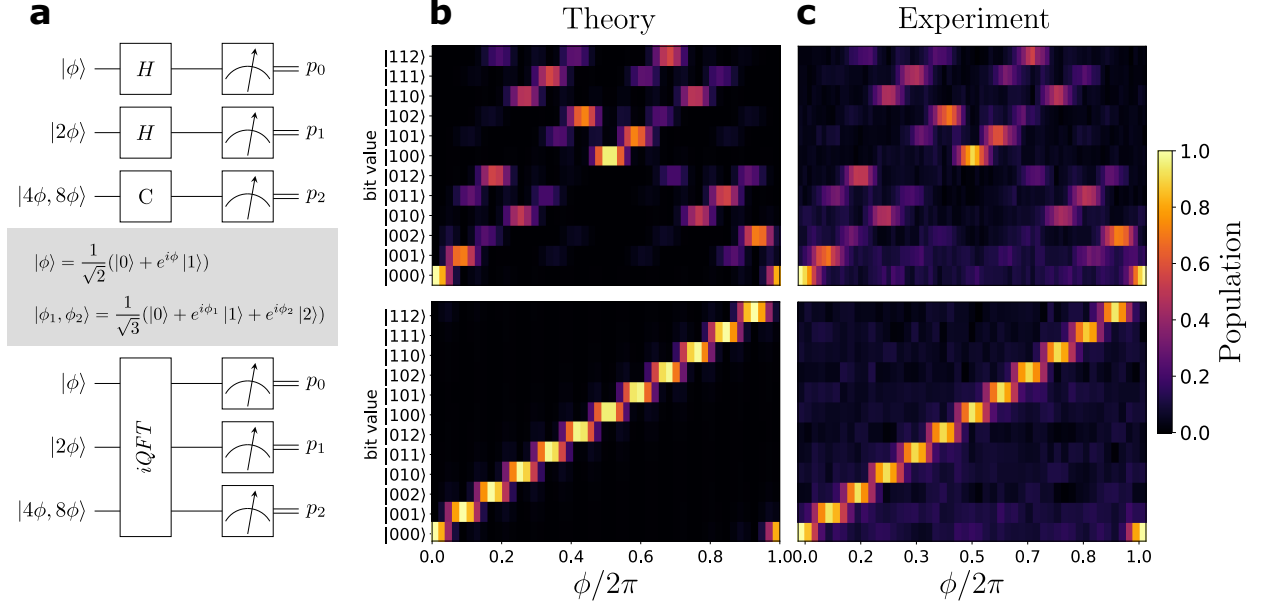


FIG. 2. Measurement outcome of the register after QFT . (a) Quantum circuits of two readout methods of register prepared in arbitrary phase state $|\Psi\rangle = |\phi\rangle \otimes |2\phi\rangle \otimes |4\phi, 8\phi\rangle$. The upper circuit maps of the phase basis onto the population basis using local single qubit (qutrit) Hadamard gates, whereas the lower one uses QFT^\dagger . (b) and (c) are results of theoretical calculations and experimental realization of the circuits on our system. Results of the experiment are in excellent agreement with calculations of the circuit output. Notably in the QFT^\dagger case there is no ambiguity between regions of phase $0 - \pi$ and $\pi - 2\pi$. Additionally the QFT^\dagger prepares final states which are close to the eigen states of the register, minimizing the loss of purity due to dephasing.

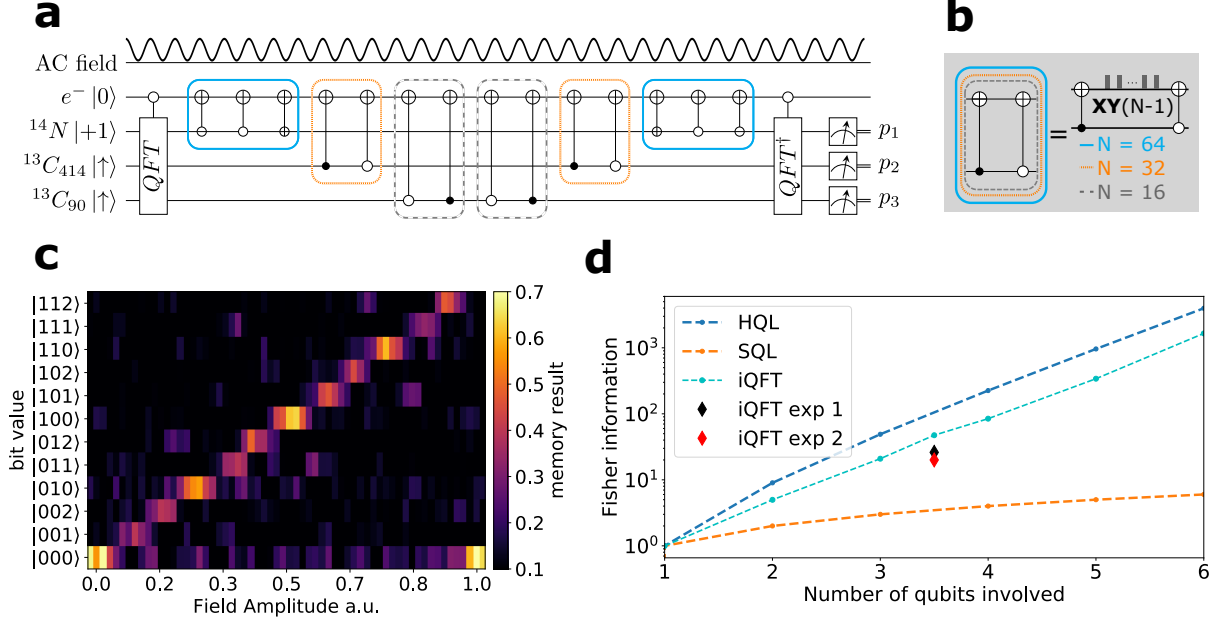


FIG. 3. (a) Sensing of an external RF field with the QFT . Usage of multiple register qubits allows to enhance the dynamic range of the sensor using multiple interrogation times, (b) Schematic representation of the quantum circuit which serves for detection of the artificial field (c) Measurement outcome of the memory registers (d) Fisher information estimated for the case of the inverse Quantum Fourier Transform (QFT^\dagger) sensing protocol, the Heisenberg scaling limit and the Standard Quantum Limit (SQL). Cyan points connected by the thin dashed line marks a simulation of the QFT^\dagger on the n -qubit circuit. Black and Red diamond are experimental results of the bare QFT^\dagger algorithm and the QFT^\dagger with sensing steps.

